



THE ANGLO-AUSTRALIAN PLANET SEARCH XXIV: THE FREQUENCY OF JUPITER ANALOGS

ROBERT A. WITTENMYER^{1,2,3}, R. P. BUTLER⁴, C. G. TINNEY^{1,2}, JONATHAN HORNER^{2,3}, B. D. CARTER³, D. J. WRIGHT^{1,2},
H. R. A. JONES⁵, J. BAILEY^{1,2}, AND SIMON J. O'TOOLE⁶

¹School of Physics, University of New South Wales, Sydney 2052, Australia; rob@unsw.edu.au

²Australian Centre for Astrobiology, University of New South Wales, Sydney 2052, Australia

³Computational Engineering and Science Research Centre, University of Southern Queensland, Toowoomba, Queensland 4350, Australia

⁴Department of Terrestrial Magnetism, Carnegie Institution of Washington, 5241 Broad Branch Road, NW, Washington, DC 20015-1305, USA

⁵Centre for Astrophysics Research, University of Hertfordshire, College Lane, Hatfield, Herts AL10 9AB, UK

⁶Australian Astronomical Observatory, P.O. Box 915, North Ryde, NSW 1670, Australia

Received 2015 December 20; accepted 2016 January 20; published 2016 February 24

ABSTRACT

We present updated simulations of the detectability of Jupiter analogs by the 17-year Anglo-Australian Planet Search. The occurrence rate of Jupiter-like planets that have remained near their formation locations beyond the ice line is a critical datum necessary to constrain the details of planet formation. It is also vital in our quest to fully understand how common (or rare) planetary systems like our own are in the Galaxy. From a sample of 202 solar-type stars, and correcting for imperfect detectability on a star-by-star basis, we derive a frequency of $6.2_{-1.6}^{+2.8}\%$ for giant planets in orbits from 3 to 7 au. When a consistent definition of “Jupiter analog” is used, our results are in agreement with those from other legacy radial-velocity surveys.

Key words: planetary systems – techniques: radial velocities

1. INTRODUCTION

Much attention has been brought to bear in recent years on the occurrence rate of Earth-like planets (e.g., Wittenmyer et al. 2011a; Howard et al. 2012; Kopparapu 2013). This is due in large part to the flood of data from the *Kepler* spacecraft mission, which has provided evidence that small planets are exceedingly common (e.g., Dressing & Charbonneau 2015; Fressin et al. 2013; Burke et al. 2015). These findings are a critical step toward answering the fundamental question “how common are planetary systems like our own solar system?” However, to fully understand the degree to which our solar system is unusual, we must also consider the other planets therein. In other words, how common are planetary systems that feature distant giant planets such as our own gas and ice giants (Jupiter, Saturn, Uranus, and Neptune). The other half of the problem, then, requires understanding the frequency and properties of planets like our own Jupiter.

One can argue that Jupiter, as the most massive and dynamically dominant body, is a key component that makes our solar system what it is today. Jupiter, as the most massive and dynamically dominant body, has played a pivotal role in shaping our solar system into what we see today. That influence can be seen in many ways when one examines the modern day solar system. The asteroid belt, interior to Jupiter’s orbit, has been sculpted over the past four and a half billion years to display intricate fine structure. The bulk of that structure is the direct result of perturbations from Jupiter, and, to a lesser extent, Saturn. Jupiter also acts to control the flux of small bodies to the inner solar system, acting to perturb asteroids and comets onto Earth-crossing orbits (e.g., Laakso et al. 2006; Horner & Jones 2008, 2012). Jupiter also hosts a large population of Trojan asteroids (Fornasier et al. 2007; Horner et al. 2012; Vinogradova & Chernetenko 2015) and irregular satellites, both of which are thought to have been captured during the giant planet’s migration (e.g., Sheppard & Jewitt 2003; Morbidelli et al. 2005; Jewitt & Haghighipour 2007; Lykawka & Horner 2010). The planet has even

been put forward as having played a key role in the volatilization of the terrestrial planets, driving the injection of a late veneer of volatile material to the inner solar system (Owen & Bar-Nun 1995; Horner & Jones 2010), and helps to drive periodic climate change on the Earth, in the form of the Milankovitch cycles (Hays et al. 1976; Horner et al. 2015).

Given Jupiter’s importance in the creation of the solar system as we observe it—the only planetary system known to host life—it is clearly important to constrain the frequency of Jupiter analogs when studying the question of our solar system’s ubiquity. In estimating the frequency of Jupiter-like planets in Jupiter-like orbits, we must first define a “Jupiter analog.” A reasonable and physically motivated definition is as follows: a gas-giant planet that plays a similar dynamical role to our own Jupiter, and that lies beyond the ice line.

The first criterion sets a lower bound on the planetary mass—a Saturn mass ($0.3 M_{\text{Jup}}$) is a reasonable limit, though, in practice, the sensitivity of Doppler radial-velocity surveys at present obviates the need to set an explicit lower bound here. A Saturn-mass planet in a 10-year orbit about a solar-type star has a velocity amplitude of 4 m s^{-1} , a signal currently at the edge of detectability for long-running “legacy” radial-velocity surveys, which have a typical velocity precision of $2\text{--}3 \text{ m s}^{-1}$ per epoch. A more physically motivated lower mass boundary may be half of a Saturn mass ($\sim 0.15 M_{\text{Jup}}$), corresponding to the overturn in the frequency of impacts that would be experienced by an Earth-like planet from a regime increasing with Jupiter-mass to one decreasing (Horner & Jones 2008, 2009). We set an upper mass limit of $13 M_{\text{Jup}}$, consistent with the accepted boundary between planets and brown dwarfs.

The second criterion ensures that such a planet has not migrated significantly beyond its formation location, leaving dynamical room for interior potentially rocky, habitable planets. This sets an inner limit of $\sim 3 \text{ au}$, which has been used by previous studies of Jupiter analogs (Wittenmyer et al. 2014a; Rowan et al. 2016). Giant planets that stay beyond this point should not prevent the accretion of telluric worlds. Finally, we require such a planet to have a low eccentricity

Table 1
Jupiter Analogs from the AAPS Sample^a

Planet	Period (days)	T_0 (BJD-2400000)	e	ω (degrees)	K (m s^{-1})	$M \sin i$ (M_{Jup})	a (au)	Reference
HD 142 c	6444 ± 144	50624 ± 168	0.32 ± 0.05	283 ± 8	60.7 ± 3.7	6.03 ± 0.48	7.27 ± 0.19	Wittenmyer et al. (2012)
HD 70642 b	2167 ± 21	51853 ± 177	0.068 ± 0.039	295 ± 29	27.8 ± 1.1	1.82 ± 0.11	3.33 ± 0.05	Carter et al. (2003)
HD 30177 b	2514.5 ± 7.7	51388 ± 19	0.21 ± 0.02	21 ± 3	133.7 ± 1.9	8.4 ± 0.4	3.57 ± 0.07	Butler et al. (2006)
HD 114613 b	3827 ± 105	55550.3 ± (fixed)	0.25 ± 0.08	244 ± 5	5.52 ± 0.40	0.48 ± 0.04	5.16 ± 0.13	Wittenmyer et al. (2014a)
HD 134987 c	5000 ± 400	51100 ± 600	0.12 ± 0.02	195 ± 48	9.3 ± 0.3	0.82 ± 0.03	5.8 ± 0.5	Jones et al. (2010)
HD 154857 c	3452 ± 105	55219 ± 375	0.06 ± 0.05	352 ± 37	24.2 ± 1.1	2.58 ± 0.16	5.36 ± 0.09	Wittenmyer et al. (2014a)
HD 160691 c	4163 ± 99	52513 ± 62	0.029 ± 0.024	23 ± 48	23.2 ± 0.5	2.00 ± 0.10	5.3 ± 0.1	McCarthy et al. (2004)
GJ 832 b	3657 ± 104	54194 ± 197	0.08 ± 0.06	246 ± 22	15.4 ± 0.7	0.68 ± 0.09	3.56 ± 0.28	Wittenmyer et al. (2014b)

Note.

^a Those 202 stars with $N > 30$ and $T_{\text{obs}} > 8$ years.

($e \lesssim 0.3$), indicating that the system has had a relatively benign dynamical history, preserving any interior rocky planets. Table 1 gives a list of Jupiter analogs in the AAPS according to this definition.

The occurrence rate of Jupiter analogs has been estimated from radial-velocity surveys (e.g., Cumming et al. 2008; Wittenmyer et al. 2014a; Rowan et al. 2016) and from microlensing (Gould et al. 2010). The former studies have generally arrived at a Jupiter-analog frequency of $\sim 3\%$ – 4% (agreeing with each other within uncertainties) while the latter arrived at a solar system analog frequency of $\sim 17\%$ based on one detection of a Jupiter/Saturn analog pair. As the temporal duration of radial-velocity survey baselines has increased, we are beginning to be able to access orbits with semimajor axes of $a \gtrsim 6$ – 8 au. At the same time, advanced direct-imaging instruments such as the Gemini Planet Imager and VLT/SPHERE are now able to probe inward of ~ 10 au (Vigan et al. 2015; Zurlo et al. 2015), the coming decade will see great advances in our understanding of not only the frequency, but also the properties of Jupiter-like planets in Jupiter-like orbits.

In this paper, we expand on our work in Wittenmyer et al. (2011b), adding a further five years of observational data from the Anglo-Australian Planet Search (AAPS), which has now been in continuous operation for 17 years. This allows us to deliver a refined estimate of the occurrence rate of Jupiter analogs in our sample. Section 2 describes the input data properties and numerical methods. Results are given in Section 3, and, in Section 4, we give our conclusions.

2. OBSERVATIONS AND COMPUTATIONAL METHODS

The AAPS has been in operation since 1998 January, and monitored about 250 stars for the first 14 years. Since 2013, the AAPS has refined its target list to the ~ 120 stars most amenable to the detection of Jupiter analogs. This is in response to simulation work in Wittenmyer et al. (2011b; 2013a), which identified the most favorable and most active stars. Increasingly limited telescope time also required the AAPS to drop targets that had too few observations to “catch up.” The AAPS has achieved a long-term radial-velocity precision of 3 m s^{-1} or better since its inception, which enables the detection of long-period giant planets. Indeed, the detection of such planets is a strength of the AAPS; of the 40 planets discovered by the AAPS, 16 (40%) have orbital periods longer than 1000 days.

To determine the underlying frequency of Jupiter analogs (defined above as planets with $a > 3 \text{ AU}$, $m \sin i > 0.3 M_{\text{Jup}}$, and $e \lesssim 0.3$), we apply the selection criteria used in

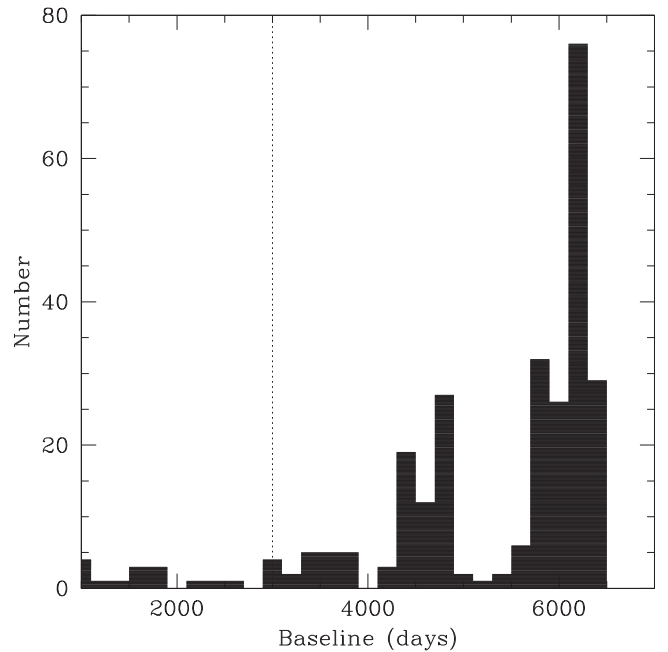


Figure 1. Histogram of observational baselines for 271 stars from the AAPS. The majority of our targets have been observed for at least 6000 days (i.e., > 16.4 years). The vertical dashed line shows our requirement of at least 3000 days of data for this analysis.

Wittenmyer et al. (2011b). That is, we only consider those AAPS targets that have more than eight years of data and at least $N = 30$ observations. The first criterion ensures that there is a sufficient observational baseline to detect a Jupiter analog through its complete orbit, and the second criterion improves the reliability of the false-alarm probability (FAP) estimation used in our detection-limit technique. Figure 1 shows a histogram of the time baselines for all 271 AAPS stars; nearly all have $T_{\text{obs}} > 3000$ days and most have $T_{\text{obs}} > 6000$ days. After applying the selection criteria above, we have 202 AAPS stars that will constitute the Jupiter-analog sample hereafter. Table 2 summarizes the data characteristics for these 202 stars. For those stars with long-term trends, a linear or quadratic fit was removed from the data before subjecting them to our detection-limit procedure. For stars known to host a substellar companion, we fit for and removed that orbit and then performed the detection-limit computations on the residuals.

We derived detection limits using the same technique as in Wittenmyer et al. (2011b) and other work by our group (e.g.,

Table 2
Summary of Radial-velocity Data

Star	N	rms ^a (m s ⁻¹)
GJ 832	109	3.6 ^a
GJ 729	30	20.7
HD 100623	104	3.5 ^a
HD 101581	33	4.0
HD 10180	38	7.2
HD 101959	49	6.6
HD 102117	63	4.4 ^a
HD 102365	187	2.7 ^a
HD 102438	59	4.6
HD 10360	65	4.8 ^a
HD 10361	66	4.4 ^a
HD 105328	53	6.5
HD 106453	37	7.6 ^a
HD 10647	53	10.6 ^a
HD 10700	258	3.5
HD 107692	48	13.7
HD 108147	58	14.1 ^a
HD 108309	69	4.1 ^a
HD 109200	39	4.5
HD 110810	39	24.1
HD 11112	41	9.3 ^a
HD 114613	244	4.0 ^a
HD 114853	58	6.9
HD 115585	31	3.6
HD 115617	247	2.5 ^a
HD 117105	32	6.7
HD 117618	78	6.2 ^a
HD 117939	35	5.8 ^a
HD 118972	51	21.0
HD 120237	57	10.9
HD 122862	104	4.8
HD 124584	44	5.8
HD 125072	86	5.5
HD 125881	36	9.3
HD 128620	102	3.5 ^a
HD 128621	119	3.7 ^a
HD 128674	31	4.9
HD 129060	45	36.9
HD 134060	98	6.6
HD 134330	46	5.7 ^a
HD 134331	60	5.5 ^a
HD 13445	72	6.1 ^a
HD 134606	66	5.4 ^a
HD 134987	77	3.4 ^a
HD 136352	169	4.7
HD 140785	40	7.1
HD 140901	117	11.4 ^a
HD 142	92	10.8 ^a
HD 143114	41	6.8
HD 144009	38	4.4
HD 144628	56	4.2
HD 145417	34	10.0
HD 146233	81	5.7 ^a
HD 146481	33	5.6
HD 147722	66	16.9 ^a
HD 147723	72	9.6 ^a
HD 149612	35	6.5
HD 150474	47	5.3
HD 151337	47	6.2
HD 153075	38	4.8
HD 154577	43	4.2
HD 154857	45	3.6 ^a
HD 155918	34	4.3
HD 155974	50	9.6

Table 2
(Continued)

Star	N	rms ^a (m s ⁻¹)
HD 156274B	96	6.5 ^a
HD 1581	117	3.7
HD 159868	86	5.8 ^a
HD 160691	180	2.4 ^a
HD 161050	31	7.6 ^a
HD 161612	52	4.5
HD 163272	40	7.0
HD 16417	121	3.9 ^a
HD 164427	44	6.2 ^a
HD 165269	33	13.5
HD 166553	43	23.4 ^a
HD 168060	48	5.8
HD 168871	73	5.0
HD 17051	37	18.2 ^a
HD 172051	63	3.8
HD 177565	106	4.0
HD 179949	66	10.9 ^a
HD 181428	45	8.6
HD 183877	45	6.0
HD 187085	74	6.1 ^a
HD 189567	94	6.1
HD 190248	235	4.0 ^a
HD 191408	185	3.9 ^a
HD 191849	42	8.9
HD 192310	161	3.1 ^a
HD 192865	45	10.5
HD 193193	54	5.6 ^a
HD 193307	83	4.5
HD 194640	83	4.7
HD 196050	56	7.8 ^a
HD 196068	35	6.6 ^a
HD 19632	30	24.8
HD 196378	51	7.1
HD 196761	49	6.5
HD 196800	41	6.7
HD 199190	55	4.9
HD 199288	83	5.2
HD 199509	33	4.7 ^a
HD 20029	36	9.8
HD 20201	35	9.3 ^a
HD 202560	47	5.0
HD 202628	30	10.9
HD 2039	46	14.0 ^a
HD 204287	48	5.2 ^a
HD 204385	43	6.6
HD 205390	36	9.6
HD 206395	45	18.5
HD 207129	124	5.2
HD 20766	57	6.7 ^a
HD 207700	36	5.0 ^a
HD 20782	57	6.1 ^a
HD 20794	145	3.6
HD 20807	99	5.0
HD 208487	49	8.2 ^a
HD 208998	36	8.3 ^a
HD 209268	30	5.5
HD 209653	42	5.3
HD 210918	72	6.1
HD 211317	44	5.3
HD 211998	47	7.4
HD 212168	51	5.6
HD 212330	33	3.8 ^a
HD 212708	37	4.5 ^a
HD 213240	37	5.5 ^a

Table 2
(Continued)

Star	N	rms ^a (m s ⁻¹)
HD 214759	32	7.1
HD 214953	84	4.9 ^a
HD 2151	172	4.7 ^a
HD 216435	78	7.1 ^a
HD 216437	56	4.7 ^a
HD 217958	37	8.2
HD 217987	42	6.0
HD 219077	72	4.9 ^a
HD 22104	43	10.9
HD 221420	86	3.9 ^a
HD 222237	34	5.6 ^a
HD 222335	30	4.5
HD 222480	33	7.4 ^a
HD 222668	36	5.8
HD 223171	63	5.8 ^a
HD 225213	35	5.4
HD 23079	40	6.6 ^a
HD 23127	44	11.6 ^a
HD 23249	93	3.2
HD 26965	111	4.5 ^a
HD 27274	30	6.9
HD 27442	103	7.3 ^a
HD 28255A	68	7.4 ^a
HD 28255B	44	15.2 ^a
HD 30177	41	9.1 ^a
HD 30295	33	9.2
HD 30876	32	7.4 ^a
HD 31527	32	6.4
HD 31827	31	8.8
HD 36108	39	4.2
HD 3823	81	5.6
HD 38283	66	4.6 ^a
HD 38382	47	5.9
HD 38973	48	5.2
HD 39091	75	5.4 ^a
HD 4308	115	4.3 ^a
HD 43834	138	5.5 ^a
HD 44120	42	3.8
HD 44447	38	5.7 ^a
HD 44594	45	5.8 ^a
HD 45289	36	7.4 ^a
HD 45701	35	5.5 ^a
HD 53705	138	4.4
HD 53706	48	3.5
HD 55693	41	6.5
HD 55720	30	3.9
HD 59468	47	4.9
HD 65907A	75	6.1
HD 67199	49	6.6 ^a
HD 67556	30	14.3
HD 69655	30	5.6
HD 70642	49	4.6 ^a
HD 70889	40	16.1
HD 72673	63	3.0
HD 72769	31	3.6 ^a
HD 73121	44	5.8
HD 73524	85	5.4
HD 74868	60	7.6
HD 75289	49	6.4 ^a
HD 7570	57	6.2
HD 76700	43	6.4 ^a
HD 78429	38	8.6
HD 80913	35	11.3 ^a
HD 83529A	32	4.7 ^a

Table 2
(Continued)

Star	N	rms ^a (m s ⁻¹)
HD 84117	145	5.6
HD 85512	31	5.0
HD 85683	30	8.8
HD 86819	36	8.7 ^a
HD 88742	36	10.1 ^a
HD 9280	33	10.3 ^a
HD 92987	52	5.3 ^a
HD 93385	46	6.9 ^a
HD 96423	42	5.3

Note.^a Velocity scatter after removal of known planets and trends.

Wittenmyer et al. 2010, 2011a; Wittenmyer & Marshall 2015). In brief, the Keplerian orbit of an artificial planet is added to the data, then we attempt to recover that signal using a generalized Lomb–Scargle periodogram (Zechmeister & Kürster 2009). A planet is considered detected if it is recovered with FAP < 1% based on the FAP estimation in Zechmeister & Kürster (2009). Comparisons of the FAP thresholds achieved by this analytic approach to those derived from a full bootstrap randomization (Kürster et al. 1997) have verified that the two methods give consistent results. We considered planets with 100 trial orbital periods between 1000 and 6000 days. The detection limit has been shown to be only minimally sensitive to small nonzero eccentricities ($e < 0.5$; Cumming & Dragomir 2010). In Wittenmyer et al. (2011b), we also derived the detection limits at $e = 0.1$ and $e = 0.2$. To illustrate the effect of (small) eccentricities on the radial-velocity amplitude K detectable in AAT data, we revisit the results of Wittenmyer et al. (2011b). Figure 2 shows the distribution of the mean detection limit \bar{K} for the 123 stars in that work (results taken from their Table 2). For $e = 0.1$, the detection limit increased by only $\sim 5\%$, while for $e = 0.2$ the limit increased by $\sim 15\%$. The typical uncertainty in \bar{K} is comparable to these eccentricity effects, and so we conclude that for the low-eccentricity orbits of Jupiter analogs (as defined above), the circular case is sufficiently informative. Hence, we consider only circular orbits in this work.

3. RESULTS

3.1. Detection Limits

Complete results for all 202 stars are given in Table 3, which shows the mean velocity amplitude \bar{K} detectable at six recovery rates: 99%, 90%, 70%, 50%, 30%, and 10%. There are substantial differences from one star to the next. We can normalize the results to each star’s intrinsic rms scatter by considering the quantity \bar{K}/rms . This allows us to express the dependence of our achieved detection limit (sensitivity) on the number of observations N —a figure of merit that can be useful in planning how many additional observations are required to obtain a robust detection (or non-detection) of a particular class of planet. Figure 4 shows the result of this exercise. We plot \bar{K}/rms versus \sqrt{N} , with the expectation that the detection limit should show a linear relationship with \sqrt{N} . In previous work on detection limits, we have required $N > 30$ based on experience with FAP computations, which become unreliable for small samples. It is evident from Figure 4 that a better

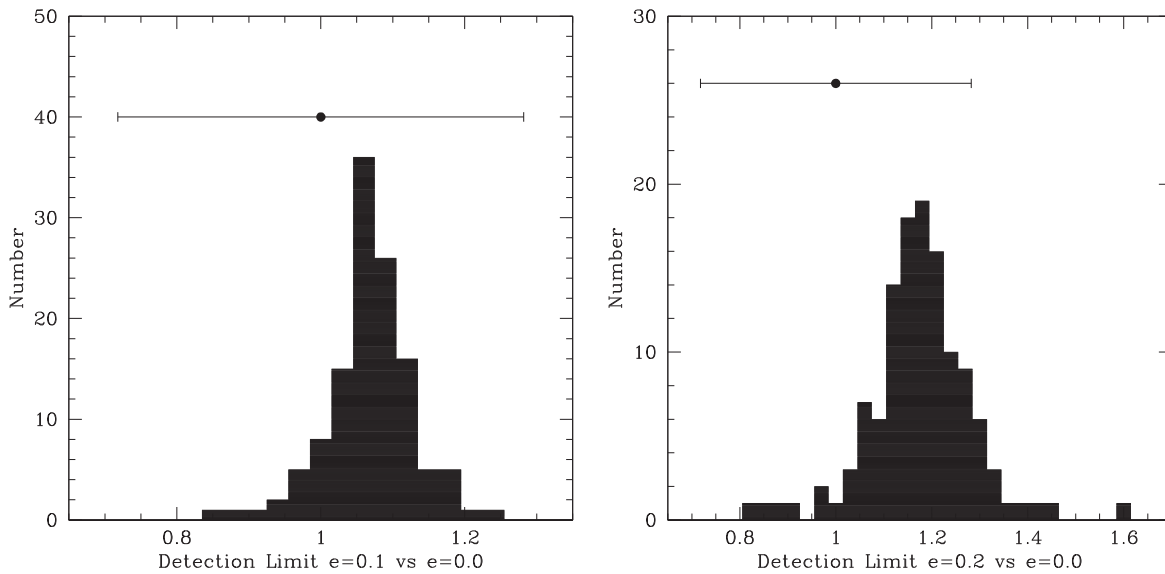


Figure 2. Distribution of mean velocity amplitude detectable at 99% confidence (\bar{K}) from Table 2 of Wittenmyer et al. (2011b). Left panel: $e = 0.1$; right panel: $e = 0.2$. The error bar represents the fractional uncertainty in \bar{K} as averaged over the trial periods from 1000 to 6000 days. For the small eccentricities considered for Jupiter analogs in this work ($e < 0.3$), the effect of eccentric orbits is within the uncertainties of \bar{K} .

choice would be $N > 40$; that is the region where the relation between normalized detection limit \bar{K}/rms and \sqrt{N} displays the expected linear relationship. We can then define the following relation for $N > 40$:

$$\frac{\bar{K}}{\text{rms}} = 2.28 \pm 0.42 - (0.093 \pm 0.036)\sqrt{N}, \quad (1)$$

where the symbols have their usual meaning. If the goal is a detection limit equal to the rms scatter of the velocity data, then approximately $N = 190$ observations would be required. As legacy radial-velocity searches such as the AAPS, Texas, and California Planet Survey (Fischer et al. 2014; Wittenmyer et al. 2014a; Endl et al. 2016) extend their time baselines toward Saturn-like orbits ($P_{\text{Saturn}} = 29$ years), then a long-term precision of 3 m s^{-1} or better is required to detect or exclude a Saturn analog ($K_{\text{Saturn}} = 3 \text{ m s}^{-1}$).

3.2. The Frequency of Jupiter Analogs

The primary aim of this work is to derive the frequency of Jupiter analogs in the AAPS sample. In this sample of 202 stars, a total of 8 Jupiter analogs (per the criteria in the Introduction) have been detected to date; their properties are enumerated in Table 1. We have excluded HD 39091b as its eccentricity $e = 0.638 \pm 0.004$ is well beyond our definition of a Jupiter analog. Such a highly eccentric planet is likely to have resulted from severe dynamical interactions (Chatterjee et al. 2008; Ford & Rasio 2008), rendering the HD 39091 system almost certainly *not* solar system-like. In addition, previous studies have shown that some such moderate-high eccentricity planets turn out, on later investigation, to be two planets on circular orbits (Wittenmyer et al. 2012, 2013b).

Following previous work (Howard et al. 2010; Wittenmyer et al. 2011a), we can use binomial statistics to estimate the frequency of Jupiter analogs in our sample. We compute the binomial probability of detecting exactly k planets in a sample of n stars, with the underlying probability p of hosting a planet. Figure 3 shows the probability distribution based on detecting

8 planets in a sample of 202 stars. This calculation yields a Jupiter analog frequency of $4.0_{-1.0}^{+1.8}\%$, where the uncertainty is the 68.3% confidence interval about the peak of the distribution. However, this calculation includes no information about the relative detectability of such planets. If Jupiter analogs were perfectly detectable for all stars in this sample, the frequency of such planets would simply be $8/202 = 4.0\%$. To compute the true underlying frequency of Jupiter analogs, we must correct the sample for incompleteness, as was done previously by Wittenmyer et al. (2011a, 2011b). This is essentially asking how many planets could have been missed. We can then adjust the binomial results above by multiplying the Jupiter analog frequency and its uncertainty by a factor $(N_{\text{detected}} + N_{\text{missed}})/N_{\text{detected}}$. Following Wittenmyer et al. (2011b), we define the survey completeness for a given radial-velocity amplitude K and period P as

$$f_c(P, K) = \frac{1}{N_{\text{stars}}} \sum_{i=1}^N f_R(P_i, K_i), \quad (2)$$

where $f_R(P, K)$ is the recovery rate as a function of K at period P , and N is the total number of stars in the sample ($N = 202$). In this way, we account for the detectabilities for each star individually, at each of the 100 trial periods. We use the specific detection limit K_P obtained for each period from the simulations described above, thus generating six pairs of (K_P , recovery fraction). Then, we generate $f_R(P, K)$ for each star by performing a linear interpolation between the six pairs of (K_P , recovery fraction). We can then estimate the recovery fraction $f_R(P, K)$ for any K . Under this scheme, an extremely stable star would have $f_R(P, K) = 1.0$, representing 100% detectability for a given (P, K) pair. Conversely, a star with poor detection limits would have a small value of $f_R(P, K)$ —approaching zero for an exceptionally “bad” star or for small K . Figure 5 shows the survey completeness obtained by summing over all 202 stars, for a range of amplitudes K from 10 to 50 m s^{-1} .

Table 3
Summary of Detection Limits: Mean Velocity Amplitude K Detectable for Orbital Periods 1000–6000 days

Star	Recovery Rate (%)					
	99	90	70	50	30	10
GJ 832	3.5 ± 1.3	2.9 ± 1.2	2.1 ± 0.9	1.5 ± 0.2	1.4 ± 0.1	1.2 ± 0.1
GJ 729	80.6 ± 43.6	79.0 ± 39.9	73.5 ± 29.9	61.6 ± 18.9	53.1 ± 14.2	45.1 ± 12.5
HD 100623	4.5 ± 0.9	4.2 ± 0.8	3.5 ± 0.7	3.1 ± 0.7	2.7 ± 0.8	2.5 ± 0.8
HD 101581	15.6 ± 6.7	13.4 ± 2.5	11.1 ± 1.3	9.5 ± 1.5	8.3 ± 1.8	7.0 ± 1.9
HD 10180	18.7 ± 4.1	17.3 ± 2.2	15.2 ± 1.2	13.6 ± 0.8	12.1 ± 1.0	10.7 ± 1.1
HD 101959	12.6 ± 1.8	11.9 ± 1.0	10.8 ± 0.6	10.1 ± 0.5	9.1 ± 0.8	8.2 ± 1.2
HD 102117	6.0 ± 2.4	5.4 ± 0.4	5.0 ± 0.3	4.5 ± 0.4	3.8 ± 0.4	3.3 ± 0.4
HD 102365	2.2 ± 0.3	2.0 ± 0.2	1.7 ± 0.2	1.5 ± 0.2	1.2 ± 0.2	1.1 ± 0.1
HD 102438	5.7 ± 0.4	5.4 ± 0.3	4.7 ± 0.4	4.3 ± 0.4	3.8 ± 0.4	3.4 ± 0.5
HD 10360	10.0 ± 1.3	9.0 ± 0.9	7.6 ± 0.7	6.2 ± 1.4	4.3 ± 2.2	3.3 ± 1.8
HD 10361	7.5 ± 0.6	6.9 ± 0.6	5.5 ± 0.5	4.8 ± 0.6	4.2 ± 0.7	3.7 ± 0.7
HD 105328	10.2 ± 0.9	9.7 ± 0.7	8.1 ± 0.7	6.6 ± 1.3	5.4 ± 1.7	4.7 ± 1.8
HD 106453	19.6 ± 4.4	18.1 ± 3.1	15.3 ± 1.9	13.2 ± 1.7	13.5 ± 7.3	10.7 ± 4.2
HD 10647	22.9 ± 5.6	18.9 ± 2.2	15.3 ± 1.4	13.4 ± 1.4	11.3 ± 1.6	9.0 ± 2.0
HD 10700	2.9 ± 0.8	2.7 ± 0.8	2.0 ± 0.6	1.5 ± 0.4	1.3 ± 0.3	1.1 ± 0.1
HD 107692	26.3 ± 2.6	24.4 ± 2.2	19.5 ± 1.8	16.8 ± 1.5	14.8 ± 1.4	13.2 ± 1.3
HD 108309	6.7 ± 0.7	6.2 ± 0.6	5.1 ± 0.4	4.4 ± 0.6	3.6 ± 0.8	3.1 ± 0.7
HD 109200	10.7 ± 1.1	10.1 ± 0.6	9.2 ± 0.5	8.7 ± 0.4	7.8 ± 0.6	6.9 ± 0.6
HD 110810	72.7 ± 23.3	68.2 ± 18.5	64.1 ± 18.4	51.8 ± 12.2	43.3 ± 7.0	36.9 ± 4.0
HD 11112	25.8 ± 4.6	23.7 ± 2.4	19.9 ± 1.6	16.2 ± 1.9	13.7 ± 2.1	11.7 ± 2.4
HD 114613	3.6 ± 0.4	3.4 ± 0.3	2.8 ± 0.4	2.4 ± 0.3	2.0 ± 0.5	1.9 ± 0.5
HD 114853	10.7 ± 1.1	9.7 ± 1.9	7.8 ± 1.0	6.3 ± 1.3	5.1 ± 1.5	4.4 ± 1.5
HD 115585	15.3 ± 6.2	14.2 ± 4.6	13.0 ± 2.6	11.1 ± 2.3	9.8 ± 2.4	8.5 ± 2.3
HD 115617	2.6 ± 0.5	2.5 ± 0.5	2.2 ± 0.4	2.1 ± 0.4	1.9 ± 0.3	1.8 ± 0.3
HD 117105	27.6 ± 15.0	25.7 ± 9.9	25.5 ± 7.7	19.8 ± 4.0	17.0 ± 4.1	14.3 ± 4.1
HD 117618	8.5 ± 1.4	7.9 ± 1.0	6.5 ± 0.7	5.5 ± 0.8	4.6 ± 0.7	4.0 ± 0.5
HD 117939	19.1 ± 3.8	17.8 ± 2.7	15.6 ± 2.1	13.2 ± 2.4	13.0 ± 1.9	11.4 ± 1.7
HD 118972	46.0 ± 10.0	41.2 ± 6.4	32.7 ± 4.0	29.5 ± 3.4	25.6 ± 4.0	20.6 ± 3.7
HD 120237	18.4 ± 1.7	17.6 ± 1.4	15.5 ± 1.0	13.5 ± 1.7	11.7 ± 2.1	10.5 ± 2.1
HD 122862	6.0 ± 2.3	5.3 ± 0.7	4.2 ± 0.5	3.4 ± 0.4	2.7 ± 0.4	2.3 ± 0.5
HD 124584	12.6 ± 1.9	11.6 ± 1.0	10.4 ± 0.7	9.5 ± 0.5	8.5 ± 0.6	7.4 ± 0.6
HD 125072	6.9 ± 3.6	6.3 ± 3.2	4.9 ± 2.8	4.7 ± 2.5	3.4 ± 2.0	2.9 ± 1.7
HD 125881	32.2 ± 6.7	29.0 ± 3.7	24.8 ± 2.7	21.3 ± 2.9	17.2 ± 2.9	14.1 ± 2.3
HD 128620	8.4 ± 6.2	5.7 ± 2.6	3.8 ± 2.3	2.8 ± 1.5	1.7 ± 1.0	1.4 ± 0.7
HD 128621	7.2 ± 3.0	6.7 ± 2.6	6.1 ± 2.4	5.3 ± 1.7	4.7 ± 1.6	3.0 ± 0.7
HD 128674	19.2 ± 9.3	17.5 ± 6.8	16.1 ± 4.6	12.6 ± 2.2	10.9 ± 2.3	9.3 ± 2.1
HD 129060	87.4 ± 7.3	81.1 ± 6.9	70.7 ± 6.8	63.4 ± 7.5	54.5 ± 9.0	46.8 ± 9.2
HD 134060	8.2 ± 3.1	7.1 ± 0.8	5.8 ± 0.6	4.6 ± 1.0	3.2 ± 0.9	2.3 ± 0.6
HD 134330	12.5 ± 1.8	11.4 ± 0.8	9.9 ± 0.7	8.7 ± 1.0	7.0 ± 1.6	5.9 ± 1.6
HD 134331	8.6 ± 0.5	8.3 ± 0.5	7.5 ± 0.4	6.8 ± 0.5	5.9 ± 0.6	5.1 ± 0.7
HD 13445	7.2 ± 1.4	6.5 ± 0.9	5.4 ± 0.7	4.5 ± 1.0	3.6 ± 1.1	2.8 ± 0.9
HD 134606	8.2 ± 1.9	7.4 ± 1.0	5.7 ± 1.1	4.9 ± 1.7	3.3 ± 1.5	2.8 ± 1.5
HD 134987	5.0 ± 1.6	4.3 ± 0.5	3.7 ± 0.3	3.3 ± 0.2	2.8 ± 0.4	2.4 ± 0.5
HD 136352	6.7 ± 1.6	6.0 ± 0.9	5.0 ± 0.6	4.4 ± 0.5	3.6 ± 0.5	3.1 ± 0.5
HD 140785	14.1 ± 2.8	13.1 ± 2.0	11.5 ± 1.3	10.3 ± 0.9	9.0 ± 0.7	7.9 ± 0.7
HD 140901	20.2 ± 4.2	17.0 ± 3.0	11.1 ± 2.8	8.7 ± 3.4	4.4 ± 2.6	3.5 ± 2.2
HD 142	14.1 ± 2.5	12.5 ± 1.2	10.7 ± 0.9	9.5 ± 0.8	8.2 ± 0.9	7.4 ± 1.1
HD 143114	16.6 ± 3.2	15.4 ± 1.8	13.6 ± 1.1	12.1 ± 1.3	11.0 ± 1.4	10.0 ± 1.5
HD 144009	12.3 ± 2.4	11.2 ± 1.5	9.7 ± 1.0	8.8 ± 1.2	7.6 ± 1.7	6.6 ± 2.0
HD 144628	6.9 ± 0.8	6.6 ± 0.7	5.7 ± 0.6	4.9 ± 0.8	4.1 ± 1.0	3.6 ± 1.0
HD 145417	36.0 ± 11.4	31.3 ± 8.0	24.9 ± 3.5	21.7 ± 2.6	19.3 ± 2.7	17.1 ± 2.9
HD 146233	8.7 ± 6.1	8.0 ± 5.6	5.9 ± 4.0	4.2 ± 2.6	3.2 ± 1.8	2.6 ± 1.3
HD 146481	17.3 ± 3.7	15.9 ± 2.6	13.7 ± 1.5	12.2 ± 1.3	10.7 ± 1.9	9.6 ± 1.9
HD 147722	23.1 ± 3.0	21.6 ± 2.5	18.8 ± 1.3	18.4 ± 3.2	15.0 ± 1.9	12.9 ± 2.2
HD 147723	11.5 ± 1.1	11.0 ± 1.0	9.9 ± 0.4	10.0 ± 1.7	8.3 ± 0.5	7.4 ± 0.7
HD 149612	15.8 ± 2.6	14.2 ± 2.0	12.0 ± 1.4	10.5 ± 1.1	9.4 ± 1.3	8.1 ± 1.2
HD 150474	11.5 ± 1.0	10.9 ± 0.9	9.7 ± 0.6	8.5 ± 0.8	6.7 ± 1.3	5.7 ± 1.5
HD 151337	11.4 ± 1.3	10.7 ± 0.9	9.7 ± 0.4	8.9 ± 0.6	8.1 ± 0.7	7.1 ± 0.6
HD 153075	13.7 ± 2.1	12.6 ± 1.6	10.8 ± 1.0	9.9 ± 0.8	9.1 ± 0.9	8.2 ± 1.0
HD 154577	8.4 ± 0.5	8.1 ± 0.5	7.3 ± 0.3	6.8 ± 0.4	6.3 ± 0.6	5.9 ± 0.7
HD 154857	8.6 ± 1.1	7.8 ± 0.9	6.6 ± 0.6	5.9 ± 0.4	5.5 ± 0.4	4.9 ± 0.5
HD 155918	15.9 ± 7.4	13.7 ± 3.7	11.9 ± 2.2	9.8 ± 1.8	9.3 ± 1.3	8.1 ± 1.4
HD 155974	17.5 ± 2.0	16.1 ± 1.2	14.0 ± 0.8	12.9 ± 0.7	11.7 ± 0.8	10.3 ± 1.0

Table 3
(Continued)

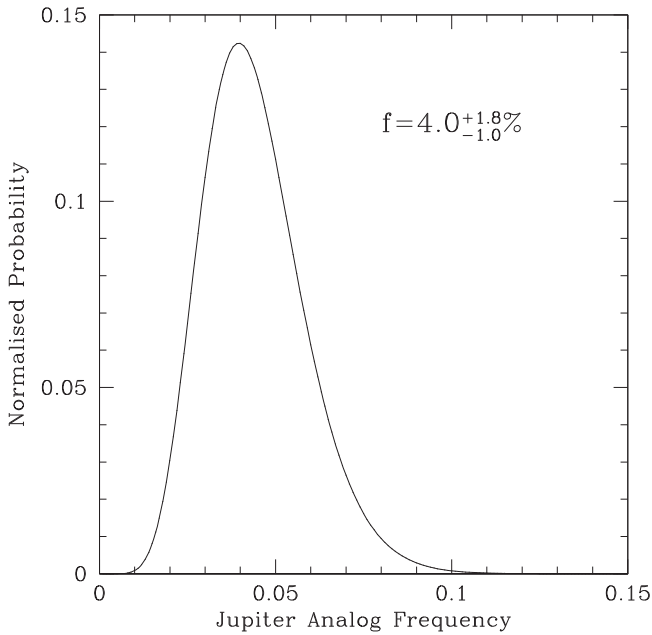
Star	Recovery Rate (%)					
	99	90	70	50	30	10
HD 156274B	9.2 ± 4.5	7.4 ± 2.6	5.5 ± 1.4	4.1 ± 1.4	2.3 ± 1.4	1.8 ± 0.9
HD 1581	4.1 ± 0.9	3.7 ± 0.7	2.9 ± 0.4	2.5 ± 0.3	2.1 ± 0.3	1.9 ± 0.2
HD 159868	7.7 ± 0.8	7.4 ± 0.8	6.9 ± 0.7	6.2 ± 0.9	5.2 ± 1.3	4.5 ± 1.4
HD 160691	2.0 ± 0.2	1.8 ± 0.2	1.6 ± 0.1	1.4 ± 0.1	1.3 ± 0.1	1.2 ± 0.1
HD 161050	45.0 ± 22.6	44.5 ± 17.2	36.0 ± 7.3	29.0 ± 5.7	24.2 ± 6.6	19.0 ± 7.7
HD 161612	7.4 ± 3.1	6.6 ± 0.4	5.8 ± 0.4	5.2 ± 0.3	4.6 ± 0.4	4.1 ± 0.6
HD 163272	19.0 ± 2.6	17.9 ± 2.2	15.1 ± 1.0	13.4 ± 1.0	12.0 ± 1.2	10.3 ± 1.5
HD 16417	5.7 ± 2.4	4.5 ± 0.6	3.7 ± 0.4	3.3 ± 0.6	2.6 ± 0.8	2.0 ± 0.6
HD 164427	15.9 ± 7.2	12.8 ± 1.9	10.6 ± 1.1	9.3 ± 1.0	8.1 ± 1.3	6.8 ± 1.2
HD 165269	48.3 ± 23.7	46.4 ± 18.8	35.6 ± 8.1	30.0 ± 6.3	22.8 ± 7.8	17.6 ± 7.1
HD 166553	54.3 ± 10.8	52.0 ± 9.9	46.6 ± 5.1	41.6 ± 3.3	37.8 ± 3.5	32.7 ± 4.1
HD 168060	10.4 ± 2.6	9.4 ± 1.4	8.0 ± 1.0	7.0 ± 0.7	6.2 ± 0.4	5.4 ± 0.4
HD 168871	7.5 ± 1.4	6.8 ± 1.0	5.4 ± 0.7	4.6 ± 0.7	4.0 ± 0.9	3.5 ± 0.8
HD 17051	55.3 ± 14.5	51.0 ± 10.3	42.3 ± 4.4	36.2 ± 3.1	31.6 ± 3.3	26.8 ± 3.2
HD 172051	10.6 ± 10.2	7.8 ± 2.7	5.9 ± 0.6	5.2 ± 0.4	4.2 ± 1.0	3.0 ± 0.9
HD 177565	6.8 ± 5.9	6.0 ± 4.3	4.7 ± 3.0	3.9 ± 2.2	3.4 ± 1.8	2.6 ± 1.3
HD 179949	19.1 ± 6.0	17.6 ± 5.2	14.2 ± 3.4	12.6 ± 5.6	8.8 ± 4.1	6.4 ± 2.9
HD 181428	16.5 ± 4.2	14.6 ± 1.2	13.0 ± 0.6	11.7 ± 0.7	10.4 ± 0.9	9.1 ± 1.1
HD 183877	11.8 ± 1.1	11.1 ± 0.7	9.7 ± 0.6	8.9 ± 0.6	8.0 ± 1.4	7.2 ± 1.8
HD 187085	7.4 ± 0.6	7.1 ± 0.4	6.6 ± 0.3	6.2 ± 0.3	5.6 ± 0.4	5.0 ± 0.5
HD 189567	7.5 ± 1.0	6.6 ± 0.6	5.5 ± 0.8	4.2 ± 1.2	3.0 ± 1.3	2.2 ± 0.9
HD 190248	4.8 ± 0.9	4.5 ± 0.8	4.0 ± 0.7	3.5 ± 0.3	3.1 ± 0.3	2.8 ± 0.4
HD 191408	4.9 ± 0.9	4.2 ± 0.4	3.5 ± 0.5	3.0 ± 0.4	2.4 ± 0.4	2.0 ± 0.4
HD 191849	16.5 ± 5.9	14.7 ± 2.1	12.6 ± 1.1	11.3 ± 1.1	9.9 ± 1.2	8.8 ± 1.5
HD 192310	2.7 ± 0.4	2.5 ± 0.3	2.1 ± 0.2	1.9 ± 0.2	1.8 ± 0.2	1.6 ± 0.2
HD 192865	23.3 ± 2.7	21.4 ± 2.1	18.0 ± 2.1	15.4 ± 1.4	13.4 ± 1.4	11.4 ± 1.6
HD 193193	9.8 ± 0.9	9.2 ± 0.6	8.0 ± 0.6	7.5 ± 0.6	6.8 ± 0.7	6.1 ± 0.6
HD 193307	7.4 ± 1.8	6.5 ± 1.1	5.6 ± 0.6	4.8 ± 0.6	3.9 ± 0.6	3.1 ± 0.4
HD 194640	7.7 ± 4.6	6.3 ± 0.9	5.4 ± 0.3	4.8 ± 0.4	4.1 ± 0.6	3.3 ± 0.6
HD 196050	12.5 ± 2.1	11.9 ± 1.8	10.6 ± 1.1	9.7 ± 0.9	8.8 ± 0.7	7.8 ± 0.7
HD 196068	21.2 ± 2.7	20.1 ± 2.0	18.0 ± 1.2	15.1 ± 2.6	14.5 ± 1.3	12.6 ± 1.7
HD 19632	82.4 ± 43.0	86.8 ± 44.2	96.6 ± 37.3	79.1 ± 29.7	61.6 ± 25.4	44.6 ± 22.7
HD 196378	14.6 ± 1.8	13.6 ± 1.0	11.8 ± 0.8	10.6 ± 0.7	9.7 ± 0.8	8.4 ± 1.0
HD 196761	13.3 ± 3.4	11.2 ± 1.7	8.5 ± 1.1	7.2 ± 1.1	5.7 ± 0.8	4.3 ± 1.1
HD 196800	17.3 ± 2.4	16.0 ± 1.2	14.2 ± 0.8	12.9 ± 0.9	11.1 ± 1.4	9.2 ± 1.8
HD 199190	8.2 ± 0.7	7.8 ± 0.5	6.8 ± 0.4	6.2 ± 0.4	5.6 ± 0.3	5.0 ± 0.4
HD 199288	8.2 ± 0.9	7.4 ± 0.8	5.8 ± 0.7	5.1 ± 0.5	4.4 ± 0.4	3.6 ± 0.4
HD 199509	19.9 ± 5.9	18.5 ± 5.0	15.4 ± 2.6	12.7 ± 1.6	10.9 ± 1.3	9.6 ± 1.5
HD 20029	42.9 ± 18.4	35.6 ± 10.5	27.0 ± 3.0	23.0 ± 2.0	20.3 ± 2.2	17.5 ± 2.8
HD 20201	29.2 ± 7.0	25.8 ± 4.2	21.6 ± 2.3	17.7 ± 1.9	16.2 ± 1.6	13.8 ± 1.7
HD 202560	10.9 ± 0.9	10.3 ± 0.7	9.2 ± 0.6	7.9 ± 1.1	6.2 ± 1.3	5.0 ± 1.4
HD 202628	51.9 ± 30.2	52.9 ± 30.3	48.6 ± 18.8	38.0 ± 9.9	31.4 ± 8.9	25.0 ± 8.4
HD 2039	34.6 ± 13.7	26.7 ± 4.8	20.4 ± 3.2	17.4 ± 3.4	15.2 ± 3.4	13.2 ± 3.5
HD 204287	11.1 ± 1.2	10.3 ± 0.7	9.1 ± 0.6	7.8 ± 1.0	5.9 ± 1.4	4.5 ± 1.0
HD 204385	14.8 ± 1.3	13.8 ± 1.1	12.0 ± 1.1	10.7 ± 1.3	9.5 ± 2.3	8.4 ± 2.5
HD 205390	34.4 ± 8.0	30.2 ± 4.2	25.3 ± 2.6	22.0 ± 2.8	17.7 ± 3.9	13.9 ± 3.8
HD 206395	39.8 ± 9.8	34.9 ± 4.5	30.5 ± 2.3	27.5 ± 2.2	24.5 ± 2.1	21.5 ± 2.3
HD 207129	7.8 ± 1.6	6.8 ± 0.9	5.4 ± 0.9	4.2 ± 1.1	2.8 ± 1.0	1.7 ± 0.3
HD 20766	10.9 ± 0.7	10.5 ± 0.6	9.5 ± 0.6	8.7 ± 0.6	7.9 ± 0.7	7.1 ± 0.5
HD 207700	15.6 ± 2.1	14.4 ± 1.5	12.8 ± 0.8	11.6 ± 0.6	10.8 ± 0.7	9.8 ± 1.0
HD 20782	10.5 ± 4.0	9.4 ± 1.2	8.4 ± 0.6	7.5 ± 0.6	6.4 ± 0.9	5.5 ± 0.9
HD 20794	3.2 ± 0.8	2.9 ± 0.4	2.6 ± 0.3	2.3 ± 0.3	2.1 ± 0.1	1.9 ± 0.1
HD 20807	8.7 ± 7.4	6.3 ± 3.4	4.4 ± 2.0	3.1 ± 1.8	2.5 ± 1.3	2.0 ± 0.9
HD 208487	17.0 ± 4.1	15.2 ± 2.9	12.6 ± 1.2	11.3 ± 1.1	10.0 ± 1.4	8.6 ± 1.8
HD 208998	20.8 ± 3.9	19.5 ± 2.4	18.3 ± 1.6	16.0 ± 1.4	14.8 ± 2.0	12.4 ± 2.4
HD 209268	22.3 ± 13.9	26.8 ± 19.2	30.9 ± 11.6	24.4 ± 3.8	19.5 ± 3.5	16.7 ± 3.3
HD 209653	13.7 ± 1.5	13.0 ± 1.2	11.6 ± 0.9	10.6 ± 0.7	9.7 ± 0.7	8.5 ± 0.8
HD 210918	8.3 ± 2.8	7.0 ± 1.6	5.3 ± 1.1	3.7 ± 1.6	1.9 ± 1.2	1.4 ± 0.6
HD 211317	13.3 ± 4.1	11.4 ± 1.2	9.7 ± 0.8	8.6 ± 1.1	7.2 ± 1.6	5.7 ± 1.5
HD 211998	21.6 ± 10.4	18.0 ± 5.9	12.8 ± 2.1	10.9 ± 1.5	8.4 ± 1.6	5.7 ± 1.8
HD 212168	10.9 ± 1.0	10.2 ± 0.8	8.4 ± 0.8	7.1 ± 0.8	6.1 ± 0.8	5.2 ± 0.8
HD 212330	14.9 ± 4.2	13.9 ± 2.7	12.4 ± 1.7	10.9 ± 1.1	9.7 ± 1.1	8.7 ± 1.4
HD 212708	15.8 ± 8.3	11.9 ± 2.5	9.8 ± 1.1	8.9 ± 1.7	8.2 ± 3.7	5.5 ± 2.5

Table 3
(Continued)

Star	Recovery Rate (%)					
	99	90	70	50	30	10
HD 213240	17.8 ± 5.5	16.4 ± 5.2	13.3 ± 1.5	11.6 ± 1.4	10.2 ± 1.6	8.7 ± 2.0
HD 214759	21.8 ± 8.8	21.4 ± 6.4	20.0 ± 3.5	16.2 ± 2.2	13.4 ± 2.9	11.3 ± 3.2
HD 214953	9.9 ± 6.1	8.1 ± 4.0	5.7 ± 1.6	4.7 ± 1.0	3.8 ± 0.9	2.7 ± 0.6
HD 2151	7.5 ± 1.7	7.1 ± 1.5	6.3 ± 1.3	5.2 ± 1.0	4.7 ± 2.0	7.3 ± 3.1
HD 216435	10.9 ± 3.8	9.2 ± 1.7	7.5 ± 1.4	6.3 ± 1.0	5.4 ± 0.8	4.6 ± 0.7
HD 216437	8.2 ± 1.2	7.6 ± 0.8	6.5 ± 0.4	5.9 ± 0.5	5.4 ± 0.6	4.9 ± 0.6
HD 217958	26.5 ± 7.1	22.9 ± 3.5	20.0 ± 1.6	17.6 ± 1.8	14.2 ± 2.9	11.5 ± 2.9
HD 219077	8.8 ± 3.7	7.5 ± 1.8	6.1 ± 0.7	5.1 ± 0.6	4.1 ± 0.6	3.2 ± 0.5
HD 22104	21.0 ± 3.8	18.7 ± 2.9	15.8 ± 1.7	14.2 ± 1.5	13.1 ± 1.7	11.5 ± 1.8
HD 221420	5.4 ± 0.5	4.9 ± 0.4	4.3 ± 0.4	3.8 ± 0.4	3.0 ± 0.7	2.4 ± 0.7
HD 222237	18.4 ± 6.2	16.6 ± 3.3	14.4 ± 1.5	11.9 ± 1.6	11.3 ± 1.2	9.9 ± 1.6
HD 222335	24.4 ± 15.1	26.5 ± 15.9	23.3 ± 6.8	18.4 ± 2.3	16.0 ± 2.2	13.6 ± 2.3
HD 222480	29.2 ± 7.7	26.8 ± 7.7	21.8 ± 4.6	17.7 ± 4.5	16.6 ± 3.5	14.1 ± 3.5
HD 222668	21.9 ± 10.5	17.6 ± 5.2	14.0 ± 2.3	11.8 ± 1.7	9.8 ± 1.4	8.1 ± 0.9
HD 223171	10.7 ± 3.4	9.1 ± 0.9	7.5 ± 0.9	6.9 ± 1.1	5.3 ± 1.2	4.5 ± 1.1
HD 225213	25.1 ± 20.0	23.0 ± 11.7	16.7 ± 4.1	15.5 ± 2.8	13.4 ± 2.4	11.4 ± 2.2
HD 23079	15.1 ± 2.6	13.6 ± 1.6	11.6 ± 1.0	10.1 ± 0.9	9.0 ± 1.0	7.9 ± 0.9
HD 23127	20.4 ± 2.6	19.6 ± 6.5	15.8 ± 2.0	13.8 ± 2.3	12.1 ± 2.7	10.5 ± 2.8
HD 23249	9.3 ± 8.9	7.6 ± 5.8	4.4 ± 0.6	3.9 ± 0.3	3.4 ± 0.3	2.9 ± 0.3
HD 26965	8.8 ± 5.1	7.2 ± 1.7	6.2 ± 1.2	5.6 ± 0.9	5.1 ± 0.7	4.6 ± 0.7
HD 27274	36.4 ± 18.5	32.1 ± 14.0	29.2 ± 10.1	23.0 ± 6.2	19.3 ± 4.9	15.6 ± 3.7
HD 27442	9.1 ± 1.1	8.5 ± 1.0	6.9 ± 0.9	5.2 ± 1.2	4.1 ± 1.3	3.5 ± 1.4
HD 28255A	14.4 ± 4.5	12.5 ± 1.6	10.2 ± 0.8	9.2 ± 0.8	7.8 ± 1.0	6.5 ± 0.9
HD 28255B	32.9 ± 2.8	30.8 ± 1.4	27.8 ± 1.1	25.1 ± 1.7	22.3 ± 3.2	20.0 ± 3.3
HD 31077	21.4 ± 4.3	19.3 ± 3.2	16.2 ± 1.4	14.0 ± 0.7	12.7 ± 1.1	10.9 ± 1.4
HD 30295	31.2 ± 14.0	29.1 ± 11.8	22.8 ± 5.6	16.3 ± 1.9	14.0 ± 2.1	11.8 ± 1.7
HD 30876	38.3 ± 18.9	34.6 ± 13.5	30.0 ± 5.7	21.1 ± 5.1	19.7 ± 3.2	16.0 ± 3.0
HD 31527	37.6 ± 20.8	30.0 ± 10.4	21.6 ± 3.6	17.6 ± 2.1	14.9 ± 2.0	11.9 ± 2.1
HD 36108	12.6 ± 3.5	11.1 ± 1.2	9.3 ± 0.7	8.1 ± 0.8	7.1 ± 1.0	5.8 ± 1.1
HD 3823	8.8 ± 2.6	7.7 ± 2.0	6.2 ± 1.3	5.3 ± 1.0	4.4 ± 0.9	3.6 ± 1.0
HD 38283	7.1 ± 0.7	6.7 ± 0.4	5.9 ± 0.4	5.4 ± 0.3	4.9 ± 0.3	4.4 ± 0.4
HD 38382	14.1 ± 4.0	12.7 ± 2.7	9.4 ± 1.3	7.7 ± 1.4	5.8 ± 1.3	4.5 ± 1.2
HD 38973	10.6 ± 1.4	9.8 ± 0.9	8.4 ± 0.6	7.3 ± 0.8	6.0 ± 0.9	4.9 ± 0.8
HD 39091	7.8 ± 1.5	7.1 ± 0.9	6.0 ± 0.6	5.1 ± 0.9	4.2 ± 0.9	3.6 ± 0.7
HD 4308	5.3 ± 1.6	4.9 ± 1.1	4.2 ± 0.9	3.2 ± 0.9	2.1 ± 0.7	1.5 ± 0.4
HD 43834	9.7 ± 3.8	9.0 ± 3.7	6.1 ± 1.7	4.4 ± 2.0	3.1 ± 1.8	2.4 ± 1.4
HD 44120	8.1 ± 0.7	7.7 ± 0.6	6.8 ± 0.4	6.1 ± 0.5	5.3 ± 0.6	4.4 ± 0.7
HD 44447	16.8 ± 3.7	15.4 ± 2.6	13.0 ± 1.1	11.0 ± 0.9	10.1 ± 0.9	8.7 ± 1.2
HD 44594	13.9 ± 5.9	11.5 ± 1.0	10.0 ± 0.8	8.9 ± 1.1	6.4 ± 2.5	5.3 ± 2.7
HD 45289	11.6 ± 1.1	10.8 ± 0.8	9.7 ± 0.6	9.7 ± 2.0	7.8 ± 0.6	6.8 ± 0.7
HD 45701	19.1 ± 5.7	17.0 ± 3.7	14.2 ± 1.4	11.7 ± 1.5	10.1 ± 1.9	8.5 ± 2.1
HD 53705	5.1 ± 1.1	4.6 ± 0.9	3.3 ± 0.5	3.2 ± 0.9	2.4 ± 0.2	2.0 ± 0.2
HD 53706	6.7 ± 0.8	6.2 ± 0.5	5.4 ± 0.3	4.9 ± 0.3	4.5 ± 0.4	4.1 ± 0.5
HD 55693	16.9 ± 1.1	15.8 ± 1.1	13.3 ± 0.9	11.5 ± 1.1	9.8 ± 1.4	8.5 ± 1.5
HD 55720	17.2 ± 9.2	17.3 ± 9.9	17.4 ± 3.9	13.7 ± 2.2	11.5 ± 2.6	10.1 ± 2.5
HD 59468	9.3 ± 0.9	8.9 ± 0.5	7.9 ± 0.5	7.1 ± 0.6	6.5 ± 0.5	6.0 ± 0.4
HD 65907A	9.1 ± 1.1	8.5 ± 1.1	6.7 ± 0.8	4.9 ± 1.4	3.5 ± 1.5	2.9 ± 1.4
HD 67199	14.0 ± 1.2	13.1 ± 1.2	11.7 ± 1.2	10.0 ± 1.4	7.7 ± 2.2	6.2 ± 2.2
HD 67556	58.3 ± 35.7	58.4 ± 34.8	64.3 ± 24.4	49.3 ± 9.9	38.8 ± 7.8	29.9 ± 7.7
HD 69655	31.3 ± 20.2	27.8 ± 13.1	25.3 ± 8.1	20.8 ± 5.2	17.9 ± 4.7	16.0 ± 4.5
HD 70642	7.5 ± 0.6	7.2 ± 0.5	6.6 ± 0.3	6.1 ± 0.4	5.5 ± 0.4	4.9 ± 0.6
HD 70889	44.0 ± 6.7	42.3 ± 11.1	34.8 ± 3.7	26.3 ± 5.8	14.9 ± 5.2	9.3 ± 2.9
HD 72673	11.5 ± 10.4	9.7 ± 7.0	7.0 ± 3.2	5.3 ± 1.4	4.2 ± 1.1	3.1 ± 0.7
HD 72769	19.5 ± 10.5	18.5 ± 7.5	14.7 ± 2.8	11.0 ± 3.0	10.4 ± 1.6	8.3 ± 1.7
HD 73121	11.2 ± 0.9	10.6 ± 0.6	9.7 ± 0.4	9.1 ± 0.5	8.2 ± 0.6	7.2 ± 0.7
HD 73524	10.4 ± 2.6	8.8 ± 1.3	6.7 ± 0.9	5.9 ± 1.4	4.2 ± 1.1	3.1 ± 1.1
HD 73526	13.9 ± 6.5	11.0 ± 2.2	8.4 ± 1.1	7.0 ± 0.9	5.9 ± 1.1	4.7 ± 1.2
HD 74868	13.7 ± 1.9	12.9 ± 1.3	11.1 ± 1.0	9.0 ± 1.6	7.0 ± 2.1	5.9 ± 2.0
HD 75289	10.3 ± 0.7	9.9 ± 0.6	9.1 ± 0.5	8.4 ± 0.8	7.6 ± 0.9	6.8 ± 1.0
HD 7570	10.6 ± 1.9	9.4 ± 0.7	7.6 ± 0.7	6.6 ± 0.5	5.9 ± 0.9	5.3 ± 1.1
HD 76700	18.2 ± 6.4	16.1 ± 5.6	12.7 ± 2.4	10.7 ± 1.7	8.9 ± 1.7	7.0 ± 1.5
HD 78429	23.6 ± 8.5	19.6 ± 3.4	15.8 ± 1.8	13.8 ± 1.7	11.5 ± 2.0	9.2 ± 1.9
HD 80913	38.6 ± 8.9	36.6 ± 7.8	31.0 ± 5.1	26.2 ± 3.9	22.3 ± 4.1	18.4 ± 4.2

Table 3
(Continued)

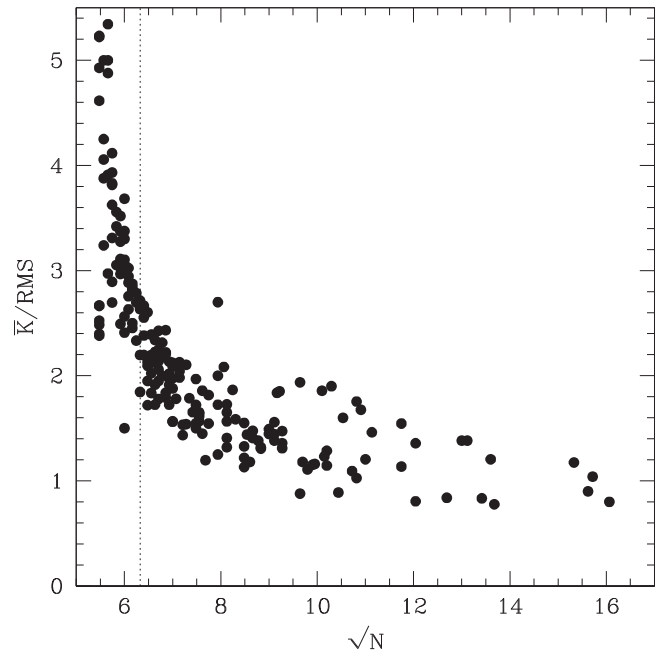
Star	Recovery Rate (%)					
	99	90	70	50	30	10
HD 83529A	24.7 ± 10.2	22.4 ± 7.9	19.1 ± 3.0	15.8 ± 1.5	13.4 ± 1.5	11.5 ± 1.7
HD 84117	7.4 ± 0.6	6.7 ± 0.5	5.6 ± 0.5	5.0 ± 0.3	4.5 ± 0.4	3.9 ± 0.5
HD 85512	19.3 ± 11.1	16.2 ± 5.6	14.0 ± 3.4	11.9 ± 2.2	10.5 ± 1.9	9.1 ± 1.8
HD 85683	41.3 ± 31.9	42.3 ± 29.3	44.1 ± 15.5	31.8 ± 5.0	25.4 ± 4.6	20.7 ± 4.5
HD 86819	23.0 ± 3.1	20.9 ± 1.9	17.6 ± 1.7	14.7 ± 2.0	12.7 ± 1.8	10.9 ± 1.6
HD 88742	30.3 ± 4.7	28.0 ± 2.4	25.4 ± 2.5	20.4 ± 3.6	17.4 ± 4.0	14.3 ± 4.0
HD 9280	50.9 ± 28.4	50.1 ± 24.8	33.7 ± 4.7	24.9 ± 4.5	22.9 ± 2.5	19.4 ± 3.2
HD 92987	7.6 ± 0.5	7.3 ± 0.4	6.7 ± 0.3	6.3 ± 0.3	5.9 ± 0.5	5.3 ± 0.7
HD 93885	14.4 ± 1.6	13.3 ± 0.9	11.6 ± 0.9	10.5 ± 0.8	9.5 ± 0.8	8.1 ± 0.9
HD 96423	11.1 ± 1.0	10.6 ± 0.7	9.6 ± 0.4	8.9 ± 0.6	8.0 ± 0.9	7.0 ± 1.1

**Figure 3.** Binomial probability density function for Jupiter analogs based on the eight detections in the 202-star AAPS sample. This yields a frequency of $f = 4.0_{-1.0}^{+1.8}\%$ (uncorrected for imperfect detectability).

The completeness fraction in Equation (2) can be used to derive a completeness correction for the published detections of Jupiter analogs in the AAPS sample. For each of the eight stars hosting a Jupiter analog (Table 1), we can compute $f_R(P, K)$ at the specific values of P and K for that known planet. All of these planets are 100% detectable based on the current AAT data for those stars. The frequency of Jupiter analogs based on this sample, corrected for completeness (detectability), is then given by

$$f_{\text{Jup}} = \frac{1}{N_{\text{stars}}} \sum_{i=1}^{N_{\text{hosts}}} \frac{1}{f_{R,i}(P_i, K_i) f_c(P_i, K_i)} = 6.2\%. \quad (3)$$

Here, $N_{\text{stars}} = 202$ total stars in the sample, $N_{\text{hosts}} = 8$ that host a Jupiter analog, and $f_R(P_i, K_i)$ refers to the recovery fractions listed above. In addition, $f_c(P_i, K_i)$ (Equation (2)) is summed over the 194 stars that did not host a Jupiter analog, to account for how detectable the eight found planets would have been around the remaining stars in the sample. We estimate from Equation (3) that 4.55 planets were “missed,” giving a completeness correction

**Figure 4.** Normalized detection limit at 99% recovery (\bar{K}/rms) vs. \sqrt{N} for our 202 stars. The dashed line indicates $N = 40$, a reasonable minimum number of observations required to obtain a detection limit that scales as the expected \sqrt{N} .

of $(N_{\text{detected}} + N_{\text{missed}})/N_{\text{detected}} = 1.56$. Hence, correcting the binomial results above yields a Jupiter analog frequency of $6.2_{-1.6}^{+2.8}\%$.

4. DISCUSSION AND CONCLUSIONS

The frequency of Jupiter analogs has been estimated by several authors using both radial-velocity and microlensing results. Our results are consistent with the literature, i.e., that Jupiter-like planets in Jupiter-like orbits are relatively uncommon, occurring around less than 10% of stars. For giant planets beyond 3 au, frequencies of $f \sim 3\%$ are reported by several teams (Cumming et al. 2008; Wittenmyer et al. 2014a; Rowan et al. 2016), with uncertainties of 1%–3%. The recent work of Rowan et al. (2016; R16), whose techniques most closely mirror our own, resulted in an estimate of $f \sim 1\%$ –4% (90% confidence interval). At first glance, this is in disagreement with our result of $6.2_{-1.6}^{+2.8}\%$. However, we note two important differences: (1) R16 defined Jupiter analogs as planets with masses 0.3 – $3 M_{\text{Jup}}$ and periods 5–15 years, and (2) they report a

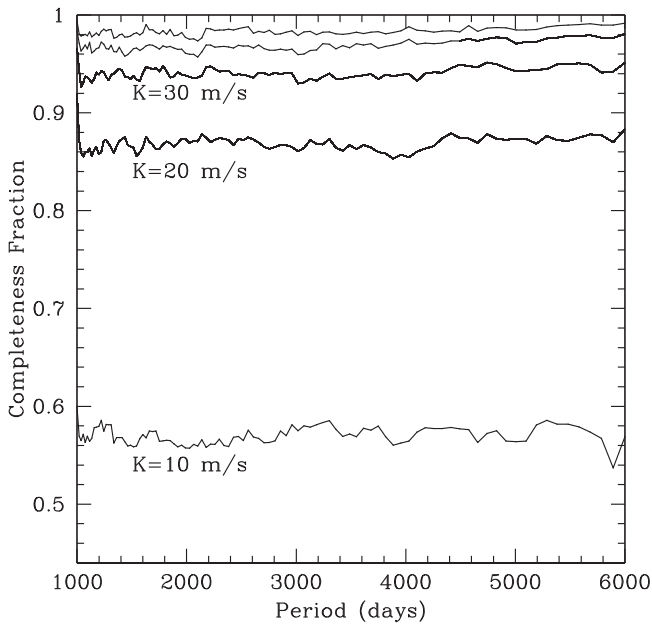


Figure 5. Completeness fraction for 202 AAPS stars, as a function of orbital period and radial-velocity amplitude K . From bottom to top, the curves are for $K = 10, 20, 30, 40,$ and 50 m s^{-1} .

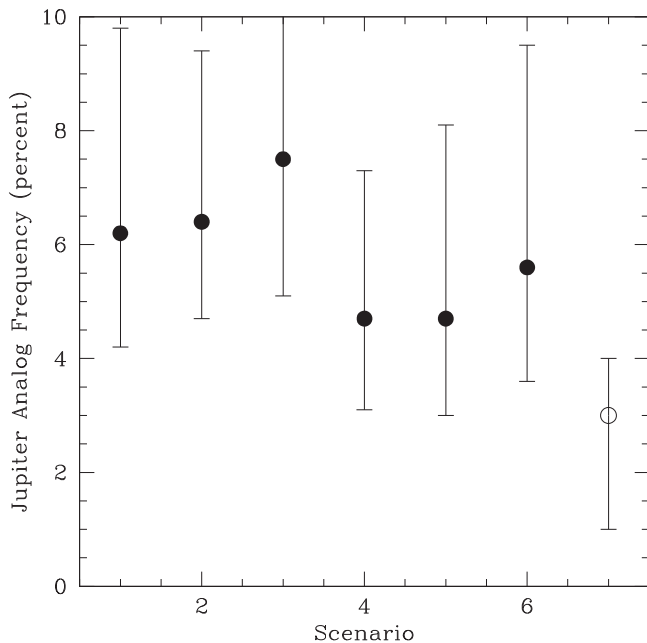


Figure 6. Frequency of Jupiter analogs as computed under various scenarios (filled circles) as compared to the result of Rowan et al. (2016) from the Lick–Carnegie survey (open circle). Scenarios 1, 2, and 3 use our definition of a Jupiter analog, while Scenarios 4, 5, and 6 use the R16 definition, which excludes planets with $P > 15$ years and $m > 3 M_{\text{Jup}}$. Error bars represent the 10%–90% confidence intervals. When consistent definitions are used, our results are in agreement with those of R16.

10%–90% confidence interval, whereas we report a 68.7% (1σ) confidence interval about the peak of the posterior distribution function. If we adopt the Jupiter analog definition of R16, HD 142c and HD 30177b no longer count, and we get a binomial probability of six detections in 202 stars as $f \sim 2.0\%–4.7\%$ (90% confidence interval). Correcting for missed planets as in Equation (3), this range becomes $f \sim 3.1\%–7.3\%$. Hence, by aligning our definitions and

reported confidence intervals, our results overlap with those of R16.

Our central value for the Jupiter analog frequency remains somewhat higher, which can be attributed to the missed-planet correction. While both this work and R16 determined survey completeness via injection and recovery simulations, R16 averaged detectability over phases at a given period, whereas our technique considered recovery as a binary function—that is, if 1 of the 30 trial phases resulted in a non-detection, the K amplitude at that period was deemed “not recovered” and K was increased until all phases resulted in a significant recovery of the injected signal. The result is that our approach would give higher (more conservative) limits and, by Equation (2), that translates into lower recovery rates for a given K , leading to a larger missed-planet correction (Equation (3)) than that derived by R16. This in turn leads to a higher Jupiter analog frequency.

We explored this further by considering a number of different subsets of our results. Figure 6 shows six possibilities, all reported as 10%–90% confidence intervals, after R16 (as noted above). The six scenarios are, from left to right: (1) our adopted result using 202 AAPS stars and our definition of Jupiter analog; (2) the same but using all 271 AAPS stars, including those with insufficient time coverage; (3) the same, but only using the 141 AAPS stars that have more than 40 observations; (4) using 202 AAPS stars but with the R16 definition of Jupiter analog; (5) using all 271 AAPS stars but with the R16 definition of a Jupiter analog; (6) using only the 141 AAPS stars with $N > 40$ and the R16 definition of a Jupiter analog. As noted above, matching the R16 definition excludes two AAPS detections and reduces the derived frequency (Scenarios 4, 5, and 6). Including all 271 AAPS stars, even those patently incapable of discerning these types of planets (too few observations, too short a baseline), we obtain the same underlying frequency. Spreading the detections over more stars in the sample is countered by the missed-planet correction of the added stars, which are assumed to add no information to the detectability. This leads to a larger missed-planet correction as per Equation (3). The effects cancel out, obviating any concern that we have somehow “cherry picked” our sample. Similarly, by intentionally choosing the more-suitable stars ($N > 40$, Scenarios 3 and 6), we again arrive at the same result but with larger uncertainties due to the smaller sample used.

Our AAPS sample contains 45 stars (22%) with linear trends or unconstrained long-period objects imposing some curvature on the radial velocities. These objects may be gas-giant planets, or low-mass stars on orbits of thousands of years. Direct imaging campaigns are revealing a population of super-Jupiter-mass objects in orbits of tens of au (e.g., Kalas et al. 2008; Marois et al. 2008; Chauvin et al. 2012), well beyond the range reasonably detectable by radial velocity. The handful of such objects now known range in orbital separation from 9 to 113 au, and in mass from 3 to $10 M_{\text{Jup}}$, though with large uncertainties correlated with the host star’s age (Rameau et al. 2013; Goździewski & Migaszewski 2014). From non-detections in the Gemini NICI planet-finding campaign, Nielsen et al. (2013) estimated that no more than 20% of B and A stars can host planets $M > 4 M_{\text{Jup}}$ between 59 and 460 au. To date, high-contrast imaging studies favor A-/B-type stars, while radial-velocity surveys traditionally prioritize solar-type FGK stars. The two techniques are looking for the same

types of objects, but there remain these gaps in both host-star-type (mass) and orbital separation due to the selection biases intrinsic to each technique. There remains no substitute for time as we seek to elucidate the properties of large-separation giant planets. Radial-velocity surveys such as the AAPS will probe toward true Saturn analogs, and imaging campaigns will reach working angles closer to their host stars, toward Jupiter-like separations (~ 5 au). Furthermore, the next generation of microlensing surveys (e.g., Lee et al. 2015) will make important contributions, being unfettered by the biases inherent to the former two methods.

J.H. is supported by USQ's Strategic Research Fund: the STARWINDS project. C.G.T. is supported by Australian Research Council grants DP0774000 and DP130102695. This research has made use of NASA's Astrophysics Data System (ADS), and the SIMBAD database, operated at CDS, Strasbourg, France. This research has also made use of the Exoplanet Orbit Database and the Exoplanet Data Explorer at exoplanets.org (Wright et al. 2011).

REFERENCES

- Burke, C. J., Christiansen, J. L., Mullally, F., et al. 2015, *ApJ*, 809, 8
- Butler, R. P., Wright, J. T., Marcy, G. W., et al. 2006, *ApJ*, 646, 505
- Carter, B. D., Butler, R. P., Tinney, C. G., et al. 2003, *ApJL*, 593, L43
- Chatterjee, S., Ford, E. B., Matsumura, S., & Rasio, F. A. 2008, *ApJ*, 686, 580
- Chauvin, G., Lagrange, A.-M., Beust, H., et al. 2012, *A&A*, 542, A41
- Cumming, A., Butler, R. P., Marcy, G. W., et al. 2008, *PASP*, 120, 531
- Cumming, A., & Dragomir, D. 2010, *MNRAS*, 401, 1029
- Dressing, C. D., & Charbonneau, D. 2015, *ApJ*, 807, 45
- Endl, M., Brugamyer, E. J., Cochran, W. D., et al. 2016, *ApJ*, 818, 34
- Fischer, D. A., Marcy, G. W., & Spronck, J. F. P. 2014, *ApJS*, 210, 5
- Ford, E. B., & Rasio, F. A. 2008, *ApJ*, 686, 621
- Fornasier, S., Dotto, E., Hainaut, O., et al. 2007, *Icar*, 190, 622
- Fressin, F., Torres, G., Charbonneau, D., et al. 2013, *ApJ*, 766, 81
- Gould, A., Dong, S., Gaudi, B. S., et al. 2010, *ApJ*, 720, 1073
- Goździewski, K., & Migaszewski, C. 2014, *MNRAS*, 440, 3140
- Hays, J. D., Imbrie, J., & Shackleton, N. J. 1976, *Sci*, 194, 1121
- Horner, J., Gilmore, J. B., & Waltham, D. 2015, arXiv:1511.06043
- Horner, J., & Jones, B. W. 2008, *IJAsB*, 7, 251
- Horner, J., & Jones, B. W. 2009, *IJAsB*, 8, 75
- Horner, J., & Jones, B. W. 2010, *IJAsB*, 9, 273
- Horner, J., & Jones, B. W. 2012, *IJAsB*, 11, 147
- Horner, J., Müller, T. G., & Lykawka, P. S. 2012, *MNRAS*, 423, 2587
- Howard, A. W., Marcy, G. W., Bryson, S. T., et al. 2012, *ApJS*, 201, 15
- Howard, A. W., Marcy, G. W., Johnson, J. A., et al. 2010, *Sci*, 330, 653
- Jewitt, D., & Haghighipour, N. 2007, *ARA&A*, 45, 261
- Jones, H. R. A., Butler, R. P., Tinney, C. G., et al. 2010, *MNRAS*, 403, 1703
- Kalas, P., Graham, J. R., Chiang, E., et al. 2008, *Sci*, 322, 1345
- Kopparapu, R. K. 2013, *ApJL*, 767, L8
- Kürster, M., Schmitt, J. H. M. M., Cutispoto, G., & Dennerl, K. 1997, *A&A*, 320, 831
- Laakso, T., Rantala, J., & Kaasalainen, M. 2006, *A&A*, 456, 373
- Lee, C.-U., Kim, S.-L., Cha, S.-M., et al. 2015, *IAUGA*, 22, 52676
- Lykawka, P. S., & Horner, J. 2010, *MNRAS*, 405, 1375
- Marois, C., Macintosh, B., Barman, T., et al. 2008, *Sci*, 322, 1348
- McCarthy, C., Butler, R. P., Tinney, C. G., et al. 2004, *ApJ*, 617, 575
- Morbidelli, A., Levison, H. F., Tsiganis, K., & Gomes, R. 2005, *Natur*, 435, 462
- Nielsen, E. L., Liu, M. C., Wahhaj, Z., et al. 2013, *ApJ*, 776, 4
- Owen, T., & Bar-Nun, A. 1995, *Icar*, 116, 215
- Rameau, J., Chauvin, G., Lagrange, A.-M., et al. 2013, *ApJL*, 772, L15
- Rowan, D., Meschiari, S., Laughlin, G., et al. 2016, *ApJ*, 817, 104
- Sheppard, S. S., & Jewitt, D. C. 2003, *Natur*, 423, 261
- Vigan, A., Bonnefoy, M., Ginski, C., et al. 2015, arXiv:1511.04076
- Vinogradova, T. A., & Chernetenko, Y. A. 2015, *SoSyR*, 49, 391
- Wittenmyer, R. A., Horner, J., Tinney, C. G., et al. 2014a, *ApJ*, 783, 103
- Wittenmyer, R. A., Horner, J., Tuomi, M., et al. 2012, *ApJ*, 753, 169
- Wittenmyer, R. A., & Marshall, J. P. 2015, *AJ*, 149, 86
- Wittenmyer, R. A., O'Toole, S. J., Jones, H. R. A., et al. 2010, *ApJ*, 722, 1854
- Wittenmyer, R. A., Tinney, C. G., Butler, R. P., et al. 2011a, *ApJ*, 738, 81
- Wittenmyer, R. A., Tinney, C. G., Horner, J., et al. 2013a, *PASP*, 125, 351
- Wittenmyer, R. A., Tinney, C. G., O'Toole, S. J., et al. 2011b, *ApJ*, 727, 102
- Wittenmyer, R. A., Tuomi, M., Butler, R. P., et al. 2014b, *ApJ*, 791, 114
- Wittenmyer, R. A., Wang, S., Horner, J., et al. 2013b, *ApJS*, 208, 2
- Wright, J. T., Fakhouri, O., Marcy, G. W., et al. 2011, *PASP*, 123, 412
- Zechmeister, M., & Kürster, M. 2009, *A&A*, 496, 577
- Zurlo, A., Vigan, A., Galicher, R., et al. 2015, arXiv:1511.04083